A Compartmental Model of Mouse Thrombopoiesis and Erythropoiesis to Predict Bone Marrow Toxicity After Internal Irradiation

Nicolas Sas*[1], Julie Rousseau*[1], Frédérique Nguyen[1], Elise Bellec[1], Erik Larrsson[2], Sonia Becavin[1], Cecilia Hindorf[1,2], Jérôme Abadie[1], Nicolas Chouin[1], and Jacques Barbet[3,4]

[1]L'UNAM Université, Oniris, AMaROC, Nantes, France; [2]Department of Medical Physics, Skåne University Hospital, Lund, Sweden; [3]CRCNA, Inserm, CNRS, Université de Nantes, UMR_S 892, Nantes, France; and [4]Arronax GIP, Saint-Herblain, France

In targeted radionuclide radiotherapy, the relationship between bone marrow (BM) toxicity and absorbed dose seems to be elusive. A compartmental model of mouse thrombopoiesis and erythropoiesis was set up to predict the depletion of hematopoietic cells as a function of the irradiation dose delivered to BM by injected radiopharmaceuticals. All simulated kinetics were compared with experimental toxicity for several stages of differentiation of the 2 hematopoietic lineages. **Methods:** C57BL/6 mice were injected either with [18]FNa (37 and 60 MBq), a bone-seeking agent, or with saline. BM mean absorbed doses were calculated according to the MIRD formalism from small-animal PET/CT images. Hematologic toxicity was monitored over time, after [18]FNa injection, by studying BM progenitors and precursors in addition to blood cells. The compartmental model takes into account the pharmacokinetics of the compound, in addition to cellular kinetics and cell radiosensitivities for the 2 studied lineages. **Results:** Because biodistribution studies showed an uptake of [18]FNa in bones, the skeleton was considered as the principal source organ of BM irradiation. The time–activity curve obtained from validated quantification of PET/CT images allowed for the calculation of mean absorbed doses to the whole BM of 2.1 and 3.4 Gy for [18]FNa injections of 37 and 60 MBq, respectively. Concerning hematologic toxicity, the model was in good agreement for the 2 absorbed doses with experimental measurements of cell depletion for platelets, progenitors, and precursors within the BM in terms of time to nadir, depletion intensity, and time to recovery. The same agreement was obtained for red blood cells and their precursors. Model predictions demonstrated that BM toxicity was in correlation with the mean absorbed dose as higher depletions at nadir and longer delays to recovery were noticed for 3.4 Gy than for 2.1 Gy. **Conclusion:** The developed compartmental model of thrombopoiesis and erythropoiesis in a BM toxicity context, after internal irradiation, allowed for the prediction of cell kinetics of BM progenitors, precursors, and mature blood cells in a dose-dependent manner. This model could therefore be used to predict hematologic toxicity in preclinical internal radiotherapy to study the dose–response relationship.

Key Words: compartmental model; hematologic toxicity; bone marrow absorbed dose; radionuclide therapy

The objective of radiotherapy is to deliver a high absorbed dose of radiation to tumors that will lead to an effective treatment outcome without causing undesired effects in healthy tissues. Because of its high radiosensitivity, the bone marrow (BM) is often considered as the dose-limiting tissue, especially in radioimmunotherapy (1,2). Indeed, ionizing radiation impairs hematopoiesis by causing direct damage to hematopoietic cells and by altering the ability of BM stroma to support blood cell production (3). For all cell lineages, the time to recovery and the depletion intensity at the nadir are dependent on the injected activity (4). This hematopoietic pathway failure could be avoided by the ability to predict the BM toxicity to better define the therapeutic window before radioimmunotherapy.

The concept of dose–effect relationship established for external-beam radiotherapy should be applicable to radioimmunotherapy. However, this relationship remains elusive in the clinic (5). Most probable reasons are dose-assessment complexity and the insufficient data obtained from patients involved in radioimmunotherapy protocols, associated with previous BM sensitization because of pretreatments (6). In this context, the prediction of ionizing radiation effects on hematopoiesis by mathematic models could help to highlight the link between dose and biologic response. To develop such a model, mice are appropriate because they allow for studying hematologic toxicity on treatment-naïve subjects and for using invasive methods to assess dosimetry. In a radioimmunotherapy context, one model was developed by Shen et al. to simulate the effects of mouse BM irradiation for platelet production considering 3 compartments: BM progenitors, precursors, and platelets (7). Simulations were compared only with experimental peripheral platelet counts. One way to improve model accuracy and robustness would be to confront simulations with experimental measurements for several differentiation stages, such as progenitors or precursors in addition to mature blood cells.

Here, we developed a model that considers physical and biologic properties of the radiopharmaceutical and simulates the hierarchical structure of the hematopoietic system. From the absorbed dose and dose rate to the BM, the model predicts platelet and red blood cell (RBC) depletions. To develop and test the model, a bone-seeking agent—[18]FNa (IBA Cisbio International)—was chosen because it eased the dose calculations and efficiently irradiated the BM. Prediction accuracy was evaluated by comparing differences observed between experimental data and the model output for BM progenitors, precursors, and mature cells.

MATERIALS AND METHODS

Experimental Induction and Analysis of Myelotoxicity

Animals. Eight-week-old female C57BL/6 mice (Janvier-Europe) were used for experiments in the Center for Research and Preclinical Investigations in accordance with the institutional guidelines of the French Ethical Committee (no. CEEA.2012.131).

[18]FNa Biodistribution Assessment and Quantitative Small-Animal PET/CT Imaging. Mice were injected intraperitoneally with 10 MBq of [18]FNa. Organs were collected after euthanasia at 1, 5, or 6 h after injection (n = 4 per analysis). Radioactivity tissue concentrations were determined using a γ counter (2470 Wizard[2]; Perkin Elmer).

All imaging procedures were performed using an Inveon small-animal PET/CT device (Siemens Preclinical Solutions) under anesthesia with 1.5% isoflurane (Centravet) and 1.0 liter of O_2 per minute. Mice were injected intraperitoneally either with 0.9% NaCl (Centravet) for the control group or with 37 or 60 MBq of [18]FNa. For all mice, either belonging to the control group or injected with [18]FNa, a CT image was acquired (80 kV, 500 μA, 320 ms). CT images were achieved using a common cone-beam reconstruction method (Siemens). For mice injected with [18]FNa, CT acquisition was followed by a PET acquisition (20 min). Images were reconstructed using the 3-dimensional ordered-subsets expectation maximization algorithm (18 iterations), followed by a fast maximum a priori probability algorithm (2 iterations). They were corrected for attenuation and scattering. Mice were imaged at different times after injection.

To quantify activity within the entire skeleton, regions of interest were first drawn by automatic thresholding based on CT Hounsfield units using the Inveon Research Workplace software (Siemens). They were then exported on registered PET images. Measured activity values were corrected to take into account the signal lost due to the partial-volume effect (8), as described in the supplemental data (supplemental materials are available at http://jnm.snmjournals.org). Time–activity curves within the whole skeleton and the femur were then derived from measurements performed on 46 mice.

BM and Blood Analyses. BM was harvested by flushing 1 femur with Dulbecco modified Eagle medium supplemented with 10% fetal bovine serum (Lonza). One to 5 thousand cells were added to the MethoCult GF M3434 methycellulose medium (StemCell Technologies) and seeded in duplicate in a humidified chamber at 37°C with 5% CO_2. Multipotential colony-forming GEMM (granulocyte, erythrocyte, monocyte, and megakaryocyte) progenitors were scored after 14 d. Identification criteria were determined according to manufacturer's recommendations.

The femurs from contralateral legs were fixed in 10% buffered formaldehyde and decalcified by continued electrolysis during 72 h before paraffin embedding. Transverse 3-μm-thick sections were stained by hematoxylin-eosin-safran to identify megakaryocytes as large and polyploid cells.

Ethylenediaminetetraacetic acid–treated blood was collected via a retro-orbital puncture. Numbers of reticulocytes, erythrocytes (RBCs), and platelets were determined using an automatic hematology analyzer (MS9-5; Melet Schloesing). Cytopenias were confirmed by counting cells in blood smears stained with May-Grünwald-Giemsa.

Compartmental Model

Model Hypotheses. Two models, 1 for thrombopoiesis and 1 for erythropoiesis, were developed. Both models were divided into 3 parts: a common part adapted from Charkes et al. (9), which simulated the [18]FNa pharmacokinetic (Fig. 1A); a second part that simulated hematopoietic cell depletions after irradiation (Fig. 1B); and a third part that described the radiation injuries on BM stroma (Fig. 1C). The second and third parts are based on a simplified representation of hematopoiesis and stromal environment as previously described by Shen et al. (7).
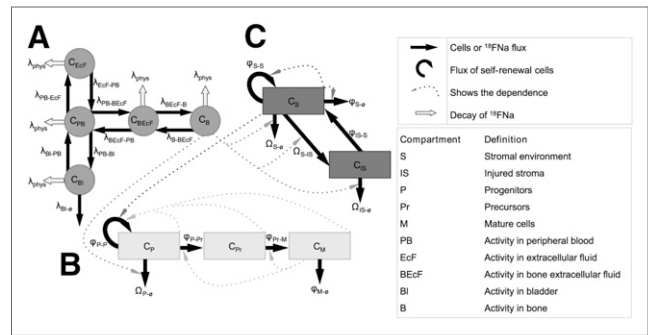

FIGURE 1. Simplified design of models for thrombopoiesis and erythropoiesis. Each model was divided into 3 parts: 1 for [18]FNa biodistribution (A), 1 for hematopoietic system of thrombopoiesis and erythropoiesis (B), and 1 for stroma (C). Solid arrows represent [18]FNa or cell flows from one compartment to another. Dashed arrows correspond to factors affecting cell flow rates. Description of each variable is given in Table 1.

Charkes model's architecture was adopted, but rate constants were adapted to mice to fit experimental biodistribution data. Shen's model was modified to take into account [18]FNa instead of [67]Cu. Modifications were also made to this model concerning the stromal damage: the stromal environment description was upgraded using the carrying capacity formulation (10).

General Description of Whole Compartmental Model. A simplified representation of the whole compartmental model is shown in Figure 1. State variables of the model are indicated in Table 1. For the whole model, the differential equation for compartment Y is described by following the general formula:

$$\frac{dC_Y(t)}{dt} = \varphi_{X-Y}(t)C_X(t) - \varphi_{Y-Z}(t)C_Y(t) - \Omega_{Y-\emptyset}(t)C_Y(t), \quad \text{Eq. 1}$$

where $\varphi_{X-Y}(t)C_X(t)$ corresponds to the compartment influx from C_X to C_Y, $\varphi_{Y-Z}(t)C_Y(t)$ describes the efflux from C_Y to C_Z, and $\Omega_{Y-\emptyset}(t)C_Y(t)$ represents elimination from compartment C_Y (excretion of [18]FNa or cell loss by radiation injuries).

Compartmental Model of [18]FNa Biodistribution. The architecture of the Charkes model was reproduced in SAAM II software (The ε Group), which generates systems of equations. The experimental blood and bone time–activity curves of the [18]FNa in mice were then implemented into SAAM II. They allowed for calculating, with the Runge-Kutta integrator, the new rate constants, which describe the variation of [18]FNa concentration in the compartments. For example, the concentration in peripheral blood (PB) was described by:

$$\frac{dC_{PB}(t)}{dt} = -(\lambda_{PB-EcF} + \lambda_{PB-BEcF} + \lambda_{PB-Bl} + \lambda_{phys})C_{PB}(t)$$
$$+ \lambda_{EcF-PB}C_{EcF}(t) + \lambda_{BEcF-PB}C_{BEcF}(t) + \lambda_{Bl-PB}C_{Bl}(t).$$
$$\text{Eq. 2}$$

The λ coefficients are rate constants, under the assumption that exchanges are linear between compartments. As described in Figure 1A, the variations correspond only to exchanges between PB and other compartments: extracellular fluid (*EcF*), bone extra cellular fluid (*BEcF*), bone (*B*), and bladder (*Bl*) and to physical decay. The same approach was used for *EcF*, *BEcF*, *Bl*, and *B*.

BM Absorbed Dose Estimation. The pharmacokinetic model allowed for deriving an accurate-fitting curve of the time–activity curve of [18]FNa in mice. According to the MIRD Committee formalism (11), the radiation dose rate within the BM as a function of time, $\dot{D}(BM, t)$, was obtained by multiplying the activity within the source region by

the S value $S(\text{BM} \leftarrow r_s)$, that is, the mean absorbed dose to BM per disintegration in the source region r_s:

$$\dot{D}(\text{BM}, t) = \sum_{\text{BM}} A(r_s, t) S(\text{BM} \leftarrow r_s). \qquad \text{Eq. 3}$$

Here, the bone was considered as the principal source of irradiation, and contributions from other organs were negligible (12). The 2 S values $S(\text{BM}_{\text{skeleton}} \leftarrow \text{skeleton})$ and $S(\text{BM}_{\text{femur}} \leftarrow \text{femur})$, which correspond respectively to the entire BM and the BM located within the femur only, were estimated using the mouse phantom MOBY with Monte Carlo calculations (MCNPX) as described previously (13). The β plus spectrum of ^{18}F available at www.doseinfo-radar.com was used for the MCNPX simulations (14). This phantom was adapted to match with the weight of the mice used experimentally (22 g; matrix, $128 \times 432 \times 128$; voxel size, 0.216 mm^3). The derived S values were $S(\text{BM}_{\text{skeleton}} \leftarrow \text{skeleton}) = 1.03 \times 10^{-2}$ mGy/(MBq·s) and $S(\text{BM}_{\text{femur}} \leftarrow \text{femur}) = 3.29 \times 10^{-1}$ mGy/(MBq·s). The mean absorbed dose to the BM at time t, $D(\text{BM}, t)$, was calculated by integrating the time-dependent dose rate from zero to t. Because all mice, including controls, underwent CT, the negligible dose contribution arising from CT was not added.

Blood cell simulations (platelets, reticulocytes, and RBCs) were obtained using the whole BM absorbed dose, whereas predictions of the cell kinetics within the BM were associated with the femoral BM absorbed dose (BM GEMM and megakaryocytes).

Hematopoietic Cell Kinetics Model. The hematopoietic differentiation stages were divided into 3 compartments according to their degree of maturity (Fig. 1B): P for BM progenitors (all stages of progenitors able to proliferate), Pr for nondividing maturing precursors (megakaryocytes or reticulocytes), and M for mature blood cells (platelets or RBCs). The hematopoietic cell kinetics model takes into account the principal regulatory mechanisms such as cell fluxes between compartments (i.e., differentiation); amplification of cell numbers (i.e., self-renewal, for progenitors only); regulatory influence of stroma and of the different cell compartments (which impact the progenitors self-renewal); and finally damage caused by radiations, modeled using the linear-quadratic hypothesis.

The cell kinetics equations were:

$$
\begin{cases}
\dfrac{dC_P(t)}{dt} = (\varphi_{P-P}(t) - \varphi_{P-Pr} - \Omega_{P-\emptyset}(t))C_P(t) \\[2mm]
\dfrac{dC_{Pr}(t)}{dt} = -\varphi_{Pr-M}\nu(t)C_{Pr}(t) + \varphi_{P-Pr}\delta(t)C_P(t) \\[2mm]
\dfrac{dC_M(t)}{dt} = -\varphi_{M-\emptyset}C_M(t) + \varphi_{Pr-M}\nu(t)C_{Pr}(t) \\[2mm]
\dfrac{dC_S(t)}{dt} = (\varphi_{S-S}(t) - \Omega_{S-\emptyset}(t) - \Omega_{S-IS}(t))C_S(t) + \varphi_{IS-S}C_{IS}(t) \\[2mm]
\dfrac{dC_{IS}(t)}{dt} = -(\varphi_{IS-S} + \Omega_{IS-\emptyset}(t))C_S(t) + \Omega_{S-IS}C_S(t),
\end{cases}
$$

$$\text{Eq. 4}$$

where $C_P(t)$, $C_{Pr}(t)$, and $C_M(t)$ are cell percentages at time t for progenitors, precursors, and mature blood cells, respectively. $C_S(t)$ and $C_{IS}(t)$ represent normal and injured stroma cells, respectively, at time t (Fig. 1C). All the other parameters, $\varphi(t)$ and $\Omega(t)$, represent the regulatory mechanisms, mentioned above, and they are thoroughly described in the supplemental data. Noticeably, they were defined within the range of potential real-life values as listed in Supplemental Table 1.

Simulations. The numeric computation of the differential equations was implemented using the Scilab 5.3.3 software (Inria, Scilab Enterprises) that uses a standard ordinary differential equation integration procedure.

TABLE 1
Compartmental Model Variables Associated with Figure 1

Quantity	Interpretation	Dimension
C_X	Content of compartment X	/
φ_{X-Y}	Cell flux from compartment X to Y	t^{-1}
λ_{X-Y}	^{18}FNa flux from compartment X to Y	t^{-1}
λ_{phys}	Radioactive decay of ^{18}FNa	t^{-1}
Ω_{X-T}	Cell loss caused by irradiation	$t^{-1}\text{MBq}^{-1}$

Statistical Analyses

Experimental measurements of hematopoietic cells were normalized to control counts for each date and are expressed as mean $\pm$ SD ($n = 8$ mice per time points). All these experiments were repeated once, except for GEMM progenitors: analyses were performed one time and confirmed by a second experiment for the nadir only.

RESULTS

Activity Quantification and Dosimetry

Results about the biodistibution study and the dosimetry calculations are given in the supplemental data. Briefly, activities measured in blood and organs were negligible as compared with activity uptake within bones (Fig. 2). These results confirmed that the skeleton could be considered as the principal source organ for BM absorbed dose calculations.

Using the derived time–activity curves, we calculated injected activities of 37 and 60 MBq of ^{18}FNa to deliver, respectively, 2.1 and 3.4 Gy to the whole BM and 2.9 and 4.7 Gy to the femoral BM.

Successful Prediction of Thrombopoiesis Kinetics Using the Compartmental Model

Mice were injected at $t = 0$ either with NaCl for the control group or with 37 or 60 MBq of ^{18}FNa. BM aplasia after irradiation increased with the absorbed dose (data not shown). Consequences on thrombocyte production were evaluated for less differentiated progenitors (GEMM) and precursors (megakaryocytes), both present in the BM and platelets in blood (Fig. 3; Table 2; Supplemental Fig. 2). Because an injected activity of ^{18}FNa leads to different absorbed doses within the BM, simulations were obtained using the BM$_{\text{femur}}$ absorbed dose for the GEMM and megakaryocytes and using the whole-BM absorbed dose for platelets.

Predictions obtained with the model were in good agreement with the experimental measures (Table 2). Simulated values of times to nadir and to recovery were within the time interval experimentally observed. Depletion intensities at nadirs were calculated with less
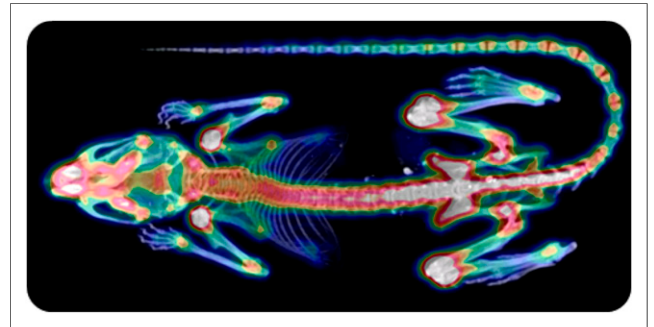

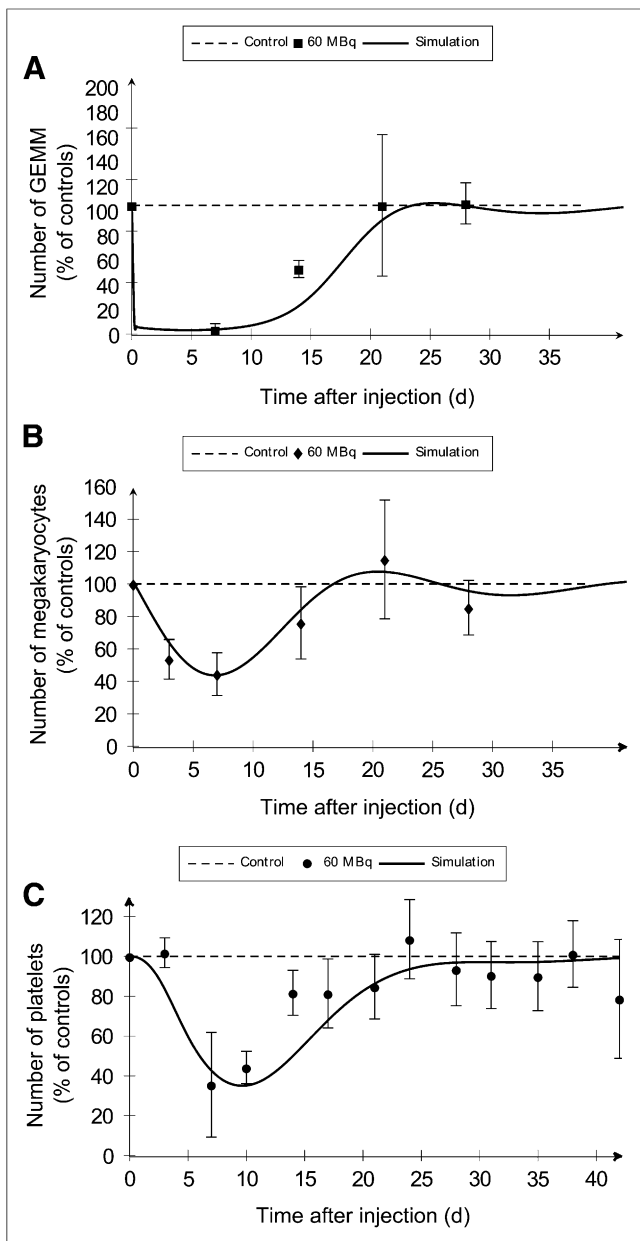**FIGURE 2.** Example of PET/CT image 1 h after injection of ^{18}FNa.

FIGURE 3. As compared with experimental measurements (dots), compartmental model simulations (solid lines) predict thrombopoietic cell kinetics after injection of 60 MBq of ^{18}FNa. (A) BM cells were isolated from femur after irradiation and cultured for GEMM progenitor colonies counting. (B) Megakaryocyte number per mm^2 within femur was determined by histology. (C) Platelets were counted in PB.

than 3% of error for GEMM and megakaryocytes and less than 6.5% for platelets.

Concerning injection of 60 MBq, simulated curves showed a rapid depletion of GEMM within the first 24 h, followed by a second slower phase reaching the nadir at day 4.8 (Fig. 3A). Megakaryocyte depletion began just after injection but was slower than the depletion observed for GEMM, with a nadir delayed in time and observed at day 7 (Fig. 3B). These effects induced a delayed decrease of platelets in blood, as demonstrated by the normal platelet count at day 3 and a nadir observed at day 9.8 (Fig. 3C).

Curve shapes were similar after injection of 37 MBq (Supplemental Fig. 2). Nevertheless, the increase of the BM absorbed

dose was associated with an increase of the depletion at the nadir for the 3 studied cell stages (Table 2). Simulated depletions were 85.5% versus 96.9% for GEMM, 39.0% versus 56.2% for megakaryocytes, and 44.5% versus 67.4% for platelets. Simulations showed no difference between 2.1 and 3.4 Gy in the time to nadir for megakaryocytes but a time lag for progenitors and platelets, because 5 more days were necessary to reach the nadir with the higher dose. Finally, significant delays for recovery were predicted by the model for GEMM and platelets (Table 2).

Prediction of Erythropoietic Toxicity by the Compartmental Model

To assess the effect of BM irradiation on erythropoiesis, RBCs and their precursors—that is, reticulocytes—were scored in blood (Fig. 4; Table 2; Supplemental Fig. 3). Associated simulations were obtained using the whole BM absorbed dose of 2.1 and 3.4 Gy for 37 and 60 MBq of ^{18}FNa, respectively.

Simulated values for times to nadir were within time intervals obtained by experimentations (Table 2). Errors between simulated nadir values and experimental percentages were less than 10%. The model predicted the observed rebounds of reticulocytes in blood with good agreement in terms of times and maximum increases. Coherent results were obtained for the simulation of recovery for the 2 cell types, except for RBC at 2.1 Gy for which a 2-d difference was observed between experimentation and simulation.

The model provided an explanation for the effects of BM irradiation on erythropoiesis. With an irradiation of 3.4 Gy, a rapid depletion of precursors within the first 72 h was noticed (Fig. 4A). As a consequence, RBCs decreased just after injection, but slower and less importantly than reticulocytes (Fig. 4B). The RBC's nadir was reached with a delay at day 16.3. The recovery of RBCs from nadir to baseline was associated with the reticulocyte rebound. The same curve shapes were obtained at 2.1 Gy (Supplemental Fig. 3).

The erythropoietic compartmental model showed that the depletion at the nadir for reticulocytes and RBCs increased with the absorbed dose (Table 2). For 2.1 and 3.4 Gy, respectively, the simulated depletions were 68.4% versus 87.5% for the precursors and 10.0% versus 16.3% for RBCs. The higher dose was associated with a faster decrease and a shift of the time to nadir. Moreover, when dose increased, the reticulocyte rebound intensity was higher and a time lag to recovery of 1.7 d was observed for both cells.

DISCUSSION

This paper presents a model that predicts platelet and RBC kinetics after ^{18}FNa administration in mice. The required dosimetric input values for this model are both the absorbed dose and the dose rate to the BM. To take into account those values, a pharmacokinetic model was developed that fit experimental biodistribution measurements performed with PET/CT imaging. This latter technique permitted the time–activity curve within the entire skeleton (rather than the measurement on an isolated and therefore nonrepresentative bone by γ counting) to be derived. The PET/CT technique also permitted evaluation of the toxicity on the same mice as the ones used for quantification. To estimate the absorbed dose and the dose rate to the BM, the S values were determined from Monte Carlo calculations using the MOBY phantom. This step is a source of uncertainties. First, the S values were phantom-based and as such not specific for each mouse. Second, the limited resolution of the MOBY phantom did not allow for an accurate representation of the BM compartments. For these 2 points, despite these limitations, the MOBY phantom corresponds up to now to the

TABLE 2

TABLE 2
Comparisons Between Experimental Data and Compartmental Model Predictions

Cell name	Dose (Gy)	Nadir				Rebound				Return to baseline (days after injection)	
		Time (days after injection)		Depletion (%)		Time (days after injection)		Maximum fold increase			
		Experimentations	Model simulation	Experimentations	Model simulation	Experimentations	Model simulation	Experimentations	Model simulation	Experimentations	Model simulation
GEMM	2.9	0–14	4	88.1	85.5	—	—	—	—	14–21	18
	4.7	0–14	4.8	96.8	96.9	—	—	—	—	14–21	23.6
Megakaryocytes	2.9	0–14	7	40.2	39.0	—	—	—	—	14–21	16.2
	4.7	3–14	7	55.5	56.2	—	—	—	—	14–21	16.8
Platelets	2.1	3–14	9.2	41.6	44.5	—	—	—	—	17–21	22
	3.4	3–14	9.8	64.4	67.4	—	—	—	—	21–24	27
Reticulocytes	2.1	0–10	2.4	70.7	68.4	10–17	6.4–15	1.4	1.5	10–17	15
	3.4	0–7	3	89.0	87.5	7–21	7.6–16.6	1.9	1.8	10–21	16.6
RBCs	2.1	0–7	5.9	12.8	10.0	—	—	—	—	7–10	12
	3.4	0–10	7.1	14.7	16.3	—	—	—	—	10–14	13.8

Data from experimentations were compared with model simulations for cellular events for 2 BM absorbed doses. For experimental data, event time values are presented as time intervals defined by experimentation sampling, and depletion percentages are given as means of irradiated mice normalized to controls.

state-of-the-art dosimetry. Finally, a uniform activity distribution within bones was considered, whereas PET images showed a higher uptake within long bone epiphyses (Fig. 2). From this, we can derive that the dose distribution in BM was nonuniform. The experimental data were obtained for 2 different injected activities of the same radiopharmaceutical. We can assume that the resulting nonuniformities were equivalent for both cases and as such the importance of the nonuniform activity distribution within bones cannot be established here.

In the case of dosimetry refinement, the radiobiologic parameters α and β of the quadratic linear model could be modified to keep the good agreement between model predictions and experimental results. An additional parameter could also be added within the linear-quadratic equations, the Lea-Catcheside coefficient (G) (15), that takes into account the effect of the dose rate at which the dose is delivered on the quadratic term. Another effect of the dose–rate on the hematologic toxicity, which is the relative rate at which cells are inactivated in regards to this given cells renewal, is natively considered in the model.

The hematologic toxicity was investigated by the traditional method—that is, by assessing the number of blood cells over time after the injection of the radiopharmaceutical (16). Model predictions were in good agreement with the experiments and with the literature in terms of curve shapes and dose increase effects. Indeed, we observed as well that increasing dose was associated with a delayed nadir with higher depletion and a delayed recovery. As far as depletion magnitude is concerned, no direct comparison was possible because of few reports on BM absorbed dose in previously published studies of internal radiotherapy. Nevertheless, the obtained toxicities for the 2 BM absorbed doses used in the present study were coherent with published external-beam radiation therapy results for the different studied cells (17,18).

The kinetics of GEMM progenitors and precursors of platelets and RBCs were also investigated, and the model accurately predicted the experimental observations. These observations confirmed that BM irradiation directly injured the progenitors whereas the decrease of precursors and mature cells could be explained by the nonrenewal of naturally dying cells, as previously described (19,20). Indeed, a rapid depletion of progenitors was noticed whereas delayed effects were observed for precursors and then for blood cells.

The robustness of the model was demonstrated by its good predictions of cell kinetics at various stages of differentiation and for 2 mean absorbed doses delivered to the BM. The parameters α and β were the only ones that were adapted to improve model predictions. On the contrary, all cellular constant values, such as cell life spans or differentiation times, were fixed and derived from the literature. It
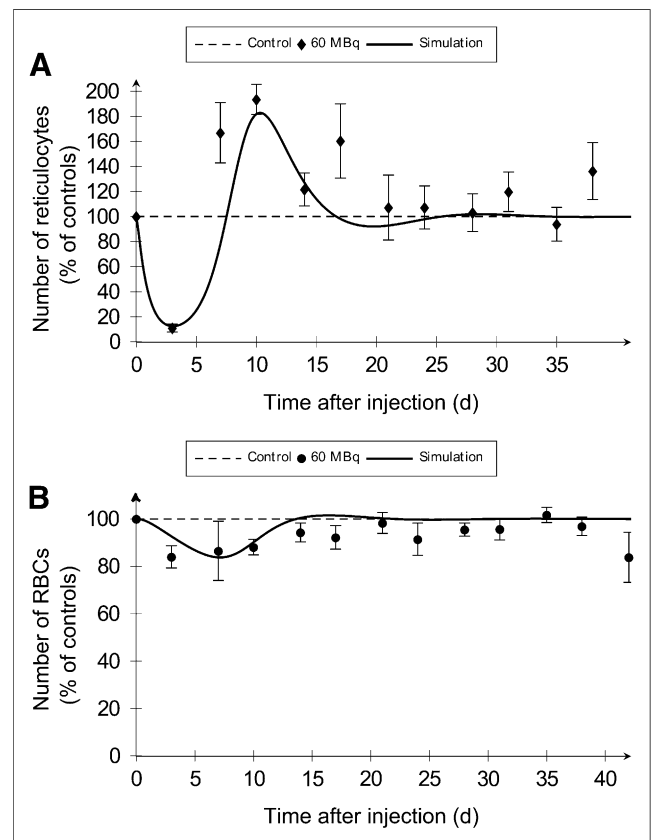

FIGURE 4. Compartmental model simulations (solid lines) of erythroid cells after BM irradiation are representative of experimental conditions (dots). Reticulocyte (A) and RBC (B) numbers in blood were determined after injection of 60 MBq of ^{18}FNa.

is important to consider that the values of α and β were still coherent with previously published values (*7*), even though those others were determined in a context of external-beam radiation therapy.

As the model predictions are based only on the absorbed dose and dose rate to the BM, we do expect that the model could be used for different radiopharmaceuticals, for instance, in a context of radioimmunotherapy, provided that the dosimetry is accurately performed. Potential applications of this model to clinical treatments are also envisaged: indirectly, by helping to improve the dose–toxicity relationship understanding, or directly, if model parameters are adapted to human constants. For this last possibility, refinements will be required to take into account, for instance, the status of BM reserve before the radioimmunotherapy protocol (*21*).

CONCLUSION

We developed a model adapted to preclinical targeted radionuclide therapy that predicted platelet and RBC toxicity in mice, with representative simulations of hematopoietic precursors, progenitors, and mature cell kinetics for 2 different levels of BM absorbed doses. This study thus opens the potential use of such models to investigate the dose–response relationships for the hematologic toxicity related to targeted radionuclide therapy.

DISCLOSURE

ACKNOWLEDGMENTS

REFERENCES

1. Sgouros G. Bone marrow dosimetry for radioimmunotherapy: theoretical considerations. *J Nucl Med.* 1993;34:689–694.
2. Hindorf C, Glatting G, Chiesa C, Linden O, Flux G. EANM dosimetry committee guidelines for bone marrow and whole-body dosimetry. *Eur J Nucl Med Mol Imaging.* 2010;37:1238–1250.
3. Carbonneau CL, Despars G, Rojas-Sutterlin S, et al. Ionizing radiation–induced expression of INK4a/ARF in murine bone marrow–derived stromal cell populations interferes with bone marrow homeostasis. *Blood.* 2012;119:717–726.
4. Larsson E, Ljungberg M, Martensson L, et al. Use of Monte Carlo simulations with a realistic rat phantom for examining the correlation between hematopoietic system response and red marrow absorbed dose in Brown Norway rats undergoing radionuclide therapy with ^{177}Lu- and ^{90}Y-BR96 mAbs. *Med Phys.* 2012; 39:4434–4443.
5. Baechler S, Hobbs RF, Jacene HA, Bochud FO, Wahl RL, Sgouros G. Predicting hematologic toxicity in patients undergoing radioimmunotherapy with ^{90}Y-ibritumomab tiuxetan or ^{131}I-tositumomab. *J Nucl Med.* 2010;51:1878–1884.
6. Siegel JA. Establishing a clinically meaningful predictive model of hematologic toxicity in nonmyeloablative targeted radiotherapy: practical aspects and limitations of red marrow dosimetry. *Cancer Biother Radiopharm.* 2005;20:126–140.
7. Shen S, DeNardo GL, Jones TD, Wilder RB, O'Donnell RT, DeNardo SJ. A preliminary cell kinetics model of thrombocytopenia after radioimmunotherapy. *J Nucl Med.* 1998;39:1223–1229.
8. Soret M, Bacharach SL. Buvat I ene. Partial-volume effect in PET tumor imaging. *J Nucl Med.* 2007;48:932–945.
9. Charkes ND, Brookes M, Makler PT. Studies of skeletal tracer kinetics: II. Evaluation of a five-compartment model of [^{18}F]fluoride kinetics in rats. *J Nucl Med.* 1979;20:1150–1157.
10. Hui C. Carrying capacity, population equilibrium, and environment's maximal load. *Ecol Modell.* 2006;192:317–320.
11. Bolch WE, Eckerman KF, Sgouros G, Thomas SR. MIRD pamphlet no. 21: a generalized schema for radiopharmaceutical dosimetry-standardization of nomenclature. *J Nucl Med.* 2009;50:477–484.
12. Czernin J, Satyamurthy N, Schiepers C. Molecular mechanisms of bone ^{18}F-NaF deposition. *J Nucl Med.* 2010;51:1826–1829.
13. Larsson E, Strand S-E, Ljungberg M, Jonsson B-A. Mouse S-factors based on Monte Carlo simulations in the anatomical realistic Moby phantom for internal dosimetry. *Cancer Biother Radiopharm.* 2007;22:438–442.
14. Stabin MG, da Luz LC. Decay data for internal and external dose assessment. *Health Phys.* 2002;83:471–475.
15. Dale RG. Dose-rate effects in targeted radiotherapy. *Phys Med Biol.* 1996;41: 1871–1884.
16. Breitz HB, Fisher DR, Wessels BW. Marrow toxicity and radiation absorbed dose estimates from rhenium-186-labeled monoclonal antibody. *J Nucl Med.* 1998;39:1746–1751.
17. Down JD, Tarbell NJ, Thames HD, Mauch PM. Syngeneic and allogeneic bone marrow engraftment after total body irradiation: dependence on dose, dose rate, and fractionation. *Blood.* 1991;77:661–669.
18. Basile LA, Gallaher TK, Shibata D, Miller JD, Douer D. Multilineage hematopoietic recovery with concomitant antitumor effects using low dose Interleukin-12 in myelosuppressed tumor-bearing mice. *J Transl Med.* 2008;6:26.
19. Ebbe S. Origin, production and life-span of blood platelets. In: Johnson SA, eds. *The Circulating Platelet.* New York, NY: Academic Press; 1971:19–43.
20. Peslak SA, Wenger J, Bemis JC, et al. Sublethal radiation injury uncovers a functional transition during erythroid maturation. *Exp Hematol.* 2011;39:434–445.
21. Siegel JA, Yeldell D, Goldenberg DM, et al. Red marrow radiation dose adjustment using plasma FLT3-L cytokine levels: improved correlations between hematologic toxicity and bone marrow dose for radioimmunotherapy patients. *J Nucl Med.* 2003;44:67–76.